Negative Thermal Transport and Giant Thermal Rectification Unveiled in a Periodic-Oscillating Temperature System

Lei Zhao, Yu Yang*, Yan Zhou*, and Lifa Zhang*

Phonon Engineering Research Center of Jiangsu Province, Ministry of Education Key Laboratory of Numerical Simulation for Large Scale Complex Systems, Center for Quantum Transport and Thermal Energy Science, Institute of Physics Frontiers and Interdisciplinary Sciences, School of Physics and Technology, Nanjing Normal University, Nanjing 210023, China

(Received 12 April 2025; accepted manuscript online 5 June 2025)

Thermal diodes, based on the thermal rectification effect, have demonstrated great promise for advanced thermal management. In previous studies, almost all thermal diodes were discussed under the condition of steady states, while the heat source of a practical thermal system often operates under dynamically fluctuating temperatures. Therefore, in this work, we employ finite element simulation to investigate transient thermal rectification behaviors in a well-built heterojunction which exhibits intrinsic thermal rectification effect under steady state. Unidirectional energy transport in the heterojunction system, decoupled from the steady-state temperature bias, is observed under a time-dependent fluctuating heat source. This phenomenon enables straightforward realization of both giant thermal rectification and negative thermal transport. Furthermore, a series of novel thermal regulation strategies are unveiled by adjusting the average temperature, frequency, and phase of the heat source. Our work not only deepens fundamental understanding of thermal regulation in time-dependent oscillating temperature systems but also uncovers many unexplored energy-saving thermal management strategies.

DOI: 10.1088/0256-307X/42/8/080702 CSTR: 32039.14.0256-307X.42.8.080702

Thermal management has become increasingly critical across various industries in recent years, spanning macroscale to microscale applications, particularly in manufacturers such as new energy vehicles,[1] high-power devices,[2–5] electronic and optoelectronic chips.[6,7] To address the growing demands of practical applications, a variety of thermal management techniques have been developed,[8–13] encompassing mainly active[14] and passive[15] heat dissipation methods. In general, active heat dissipation techniques utilize specific equipment and consume energy to facilitate heat transfer, including thermoelectric coolers,[16] heat pipes,[17] liquid cooling systems,[18] thermal transistors,[19,20] etc. Conversely, passive heat dissipation techniques rely on the intrinsic properties of materials to dissipate heat without additional energy consumption, such as heat sinks,[3,21] high thermal conductivity materials and interfaces,[22,23] thermal diodes,[24] etc. Notably, among passive heat dissipation technologies, thermal diodes have gained significant attention due to their ability to control heat flux unidirectionally without energy consumption.

At present, the realization of thermal diodes relies primarily on the non-reciprocal heat transport properties arising from the strong temperature dependent thermal conductivity of materials or physical systems.[25] By introducing asymmetric phonon spectral mismatch,[26–37] temperature dependent phase transition behaviors,[38–47] or strong temperature dependent thermal transport characteristics,[48–56] the effective thermal conductance of the overall system undergoes substantial alterations upon reversing the temperature gradient, leading to a significant thermal rectification. Originally, the concept of a thermal diode was theoretically proposed within the framework of a one-dimensional heterogeneous nonlinear atomic chain model,[25] which achieves non-reciprocal heat transport based on the asymmetric phonon spectrum and interfacial transmittance. Furthermore, the phase transition is found to significantly alter the thermal conductivity of the material, resulting in a potent thermal rectification.[38–47] A prominent example of this phenomenon is the VO_2 thermal rectifier, where the thermal conductivity changes substantially during the phase transition, achieving a thermal rectification ratio exceeding 0.5.[40] Additionally, structural phase transitions are widely utilized to control unidirectional heat transport.[45,46] Here, temperature-induced deformation triggers structural switching, thereby enabling thermal rectification. This mechanism offers the potential to achieve exceptionally high thermal rectification efficiency. However, the mechanical properties associated to this approach, particularly its susceptibility to metal fatigue over time, limit the durability of the method. It is also worth noting that thermal rectifiers based on heterojunctions have garnered considerable attention due to their simple structure, broad working temperature range, and superior performance.[52–56] These heterojunctions typically comprise two materials with op-

*Corresponding authors. Email: yuyang.njnu@foxmail.com; yan.zhou@nnu.edu.cn; phyzlf@njnu.edu.cn

© 2025 Chinese Physical Society and IOP Publishing Ltd. All rights, including for text and data mining, AI training, and similar technologies, are reserved.

posing and strongly temperature-dependent thermal conductivities (TDTCs), enabling significant variations in their effective thermal conductance under forward and reverse temperature gradients.[53,54] Therefore, the performance of such thermal rectifiers is closely related to the temperature-dependent coefficients of these heterogeneous materials. Specifically, the thermal rectification limits have been given by theoretical calculations, which are 0.5 in the linear case and 0.8 in the third-order case.[52] Simultaneously, thermal meta-materials have emerged as a powerful tool to heat transport manipulation, considering their unique capabilities in controlling heat flux (especially thermal rectification) and holding significant promise for the design and improvement of thermal diodes, thereby advancing the field of advanced cooling systems and thermal management strategies.[61,62]

Traditionally, studies on thermal rectification have mainly employed stable heat sources that are maintained at a constant temperature. However, practical industrial heat sources do not possess infinite heat capacity to ensure absolute temperature stability, leading to constant temperature fluctuations throughout the system due to environmental influence. To date, only a limited number of studies have made preliminary attempts to explore the transient heat transfer process in thermal diodes, intending to understand the impact of temperature fluctuations.[57–60] In 2017, Herrera *et al.* conducted the first investigation into the behavior of a heterojunction's response to impulse changes during the transient process using finite difference calculations.[57] They discovered that a better rectification could be achieved compared to the steady state when the time scale of thermal rectification is faster than that of thermal diffusion. Subsequently, Klinar *et al.* studied the transient temperature response of a thermal diode within a magnetocaloric refrigeration cycle and find that temperature-dependent thermal properties in thermal diodes can significantly enhance rectification efficiency, particularly under transient conditions.[58] Furthermore, Trevor *et al.*[60] explored the thermal response of heterogeneous thermal diodes with linearized TDTC and heat capacity to an imposed sinusoidal temperature boundary condition. They reveal that heterogeneous thermal diodes can achieve enhanced rectification efficiency under time-periodic temperature fields, doubling to that of steady-state conditions when at high oscillation frequency. Despite these studies demonstrating greater thermal rectification can be achieved under the transient condition, there remains a lack of systematic research exploring the influence of a fluctuating heat source on thermal rectification.

In this work, the thermal rectification performance of heterogeneous thermal diodes is explored under boundary conditions of fluctuating heat sources. Specifically, a unidirectional heat transfer phenomenon is observed, which is decoupled from the direction of the temperature gradient when subjected to a periodically oscillating heat source. Notably, a tunable thermal rectification is also achieved by adjusting the average temperature gradient, average temperature, frequency, and phase of the heat source. This adjustment results in a significant enhancement of the thermal rectification limit compared to a constant temperature heat source, without altering the fundamental composition of the thermal diode. The findings of this study provide not only novel approaches for thermal control in systems with fluctuating temperatures but also introduce innovative strategies for enhancing thermal rectification performance.

In Fig. 1(a), a structural diagram of the heterojunction-based thermal diode is presented, which consists of materials A and B, and the thermal boundary resistance (TBR) between them. Both materials A and B have a cuboid geometry, with a length ($L/2$) of 0.01 m and a square cross-section (S) with an area of 0.0004 m^2. A pair of heat sources with fluctuating temperatures are positioned at each end of the heterojunction. Temperature expression for these heat sources is provided below and illustrated in Fig. 1(b),

$$T_\mathrm{c} = T_\mathrm{c}^\mathrm{DC} + T_\mathrm{c}^\mathrm{AC} = \left(T_\mathrm{m} - \frac{\Delta T}{2}\right) + A\sin(2\pi f t), \tag{1}$$

$$T_\mathrm{h} = T_\mathrm{h}^\mathrm{DC} + T_\mathrm{h}^\mathrm{AC} = \left(T_\mathrm{m} + \frac{\Delta T}{2}\right) - A\sin(2\pi f t + \Delta\varphi), \tag{2}$$

where $T_\mathrm{h/c}$ consists of a direct current (DC) component $T_\mathrm{h/c}^\mathrm{DC}$ and an alternating current (AC) component $T_\mathrm{h/c}^\mathrm{AC}$. The subscripts h and c represent the high and low average temperatures of the heat sources, respectively. We define the forward configuration (FC) and the backward configuration (BC) based on the condition along the x-axis: $T_\mathrm{h}^\mathrm{DC} - T_\mathrm{h}^\mathrm{DC} > 0$ for the FC case and $T_\mathrm{h}^\mathrm{DC} - T_\mathrm{h}^\mathrm{DC} < 0$ for the BC case. The DC component $T_\mathrm{h/c}^\mathrm{DC}$ is composed of the midpoint of the temperature range T_m and the average temperature difference ΔT. For simplicity, $T_\mathrm{h/c}^\mathrm{AC}$ is modeled as a sine function with an amplitude A, a frequency f, and a phase difference between two heat sources $\Delta\varphi$.[60] Unless otherwise specified, f is set to 50 Hz and $\Delta\varphi$ is set to 0.

Given that the thermal rectification limit of heterojunction thermal diodes under a pair of constant-temperature heat sources has been thoroughly investigated, we directly utilize the optimal asymmetric TDTC in materials A and B to achieve a pronounced thermal rectification and amplify the impact of fluctuating heat sources. The asymmetric TDTC is represented as follows:[52]

$$\kappa_\mathrm{A}(T) = a_n \prod_{i=1}^{n} [T - (1 - A_{ni})T_\mathrm{C} - A_{ni}T_\mathrm{H}], \tag{3}$$

$$\kappa_\mathrm{B}(T) = -a_n \prod_{i=1}^{n} [T - (1 - A_{ni})T_\mathrm{H} - A_{ni}T_\mathrm{C}]. \tag{4}$$

Here, for simplicity in calculation, we set the maximum temperature T_H to be 600 K, the minimum temperature T_C as 0 K, resulting in a middle temperature T_m of 300 K. The variable n in Eqs. (3) and (4) represents the highest order of the TDTC, which is closely associated with the thermal rectification performance of the thermal diode. To ensure that the thermal conductivity is solely influenced by the highest order of TDTC, we normalize them to maintain a consistent range in TDTC. The normalized parameters are presented in Table S1 of the Supplementary Materials (SM).

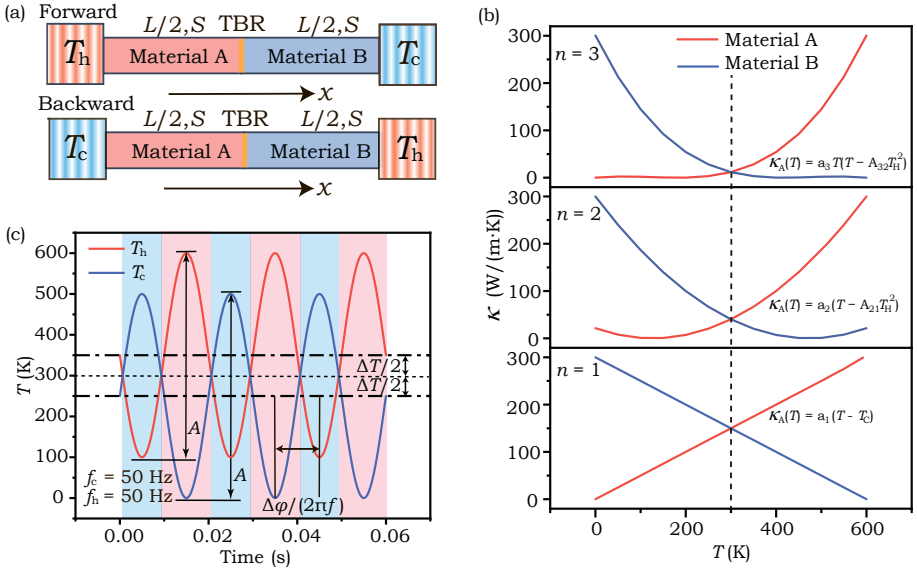

Fig. 1. (a) Schematic representation of the thermal diode heterojunction in the FC and BC cases. (b) The different highest order in asymmetrical thermal conductivities of materials A and B. (c) The adjustable periodic-oscillating temperature of AC heat sources.

In the case of a DC heat source, the temperature gradient typically extends from the high temperature heat source to the low temperature heat source. However, AC heat sources, in both FC and BC configurations, exhibit overlapping temperature fluctuations over time. In Fig. 1(c), we illustrate the temperature variations over time for both high and low temperature heat sources. The red and blue regions represent the temperature gradient along and against the x-axis, respectively. Similarly, the heat flux in the thermal diode, akin to the temperature gradient, undergoes continuous periodic variations over time. Therefore, to describe the thermal conduction characteristics of the thermal diode, once the entire system reaching a time-harmonic steady state, we calculate the average heat flux density J_{F} and J_{B} in FC and BC by statistically averaging the transient heat flux density at each moment over multiple cycles. The calculations are performed as follows:

$$J_{\mathrm{F/B}} = \frac{1}{N}\int_0^{Nt}\int_0^{L} j(x,t)\mathrm{d}x\mathrm{d}t, \tag{5}$$

where $j(x,t)$ represents the heat flux per unit area at time t and position x. And N represents the number of cycles after reaching steady state. The average heat flux density $J_{\mathrm{F/B}}$ is obtained by statistically averaging the transient heat flux density $j(x,t)$ over the entire model and multiple cycles.

Hence, the thermal rectification ratio γ and the effective thermal conductance (ETC) $G_{\mathrm{F}}^{\mathrm{eff}}$ and $G_{\mathrm{B}}^{\mathrm{eff}}$ for the FC and the BC can be accurately determined as follows:

$$\gamma = \frac{J_{\mathrm{F}}}{J_{\mathrm{B}}}, \tag{6}$$

$$G_{\mathrm{F/B}}^{\mathrm{eff}} = \frac{J_{\mathrm{F/B}}}{\Delta T}. \tag{7}$$

Furthermore, to simplify calculations, we omit the temperature dependence of heat capacity and density considering their very little changes.

Initially, we investigated the thermal rectification performance under both DC and AC heat sources. Here, the amplitude A is set to 200, and the DC temperature bias ΔT is varied continuously from 0 K to 200 K. As shown in Fig. 1(b), with an increase in the highest order n of the thermal conductivity, the effective thermal conduction decreases, and its temperature dependence becomes more significant. Consequently, in both DC and AC scenarios, we observe that the heat flux density and ETC increase with the increasing n. Furthermore, a more significant DC thermal rectification performance with increasing n is also confirmed.[52] When AC heat sources are employed instead of DC heat sources, the temperature gradient within the heterojunction oscillates sinusoidally over time, resulting in an effective average temperature gradient that surpasses those of DC heat sources. This results in an enhancement in heat flux density and ETC at FC, as illustrated in Figs. 2(a) and 2(b). Simultaneously, since the AC amplitude remains constant regardless of changes in the DC temperature difference, the additional effective temperature gradient contributed by the AC amplitude gradually diminishes with increasing DC temperature difference. This results in significant changes in heat flux density J_{F} and $G_{\mathrm{F}}^{\mathrm{eff}}$ at low DC temperature difference, as depicted in Fig. 2(b).

Upon reversing the high and low temperature heat sources, we observe a heat transport phenomenon that is distinctly different from those observed with DC heat sources, as shown in Figs. 2(c) and 2(d). In the case of DC heat sources, J_{B} remains negative and exhibits a stronger temperature difference dependence as n decreases. A remarkable phenomenon is observed in BC, where $J_{\mathrm{B}} > 0$ while $\Delta T < 0$ within a specific range. This signifies that heat flux is in the opposite direction to the temperature gradient, leading to $G_{\mathrm{B}}^{\mathrm{eff}} < 0$, as shown in Fig. 2(d). This behavior, termed negative effective thermal conductance (NETC), emerges due to the alternating transient thermal

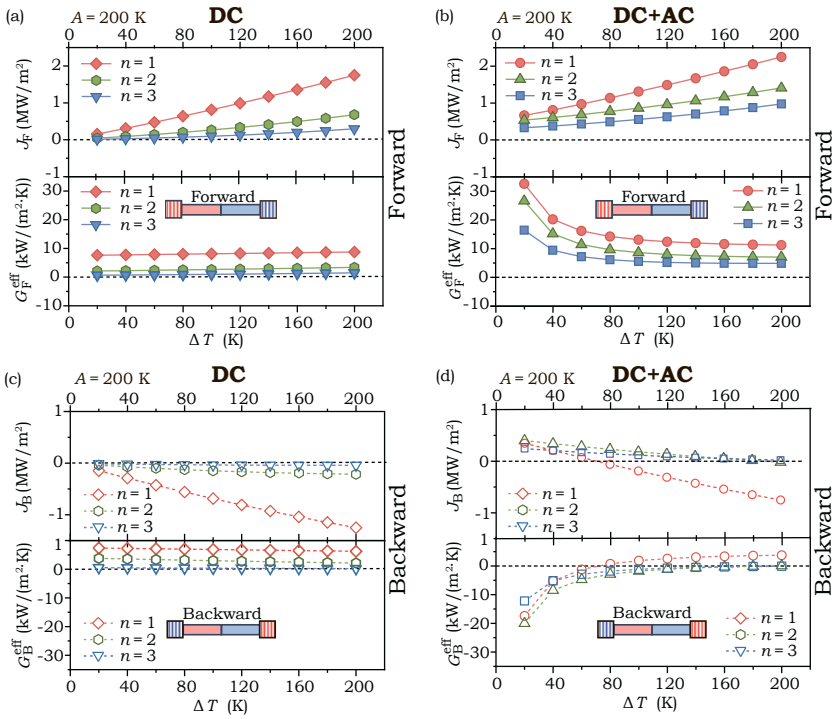

Fig. 2. The comparison of the G^{eff} and the average heat flux density J under the DC and AC+DC heat sources. The J and G^{eff} as a function of ΔT at $n = 1$, 2, and 3 under (a) DC heat sources and (b) AC+DC heat sources in the FC case. The J and G^{eff} as a function of ΔT at $n = 1$, 2, and 3 under (c) DC heat sources and (d) AC+DC heat sources in the BC case. Here, A is set as 200 K, f is set as 50 Hz, $\Delta\varphi$ is set as 0, and TBR is set as $0\,\text{m}^2\cdot\text{K/W}$.

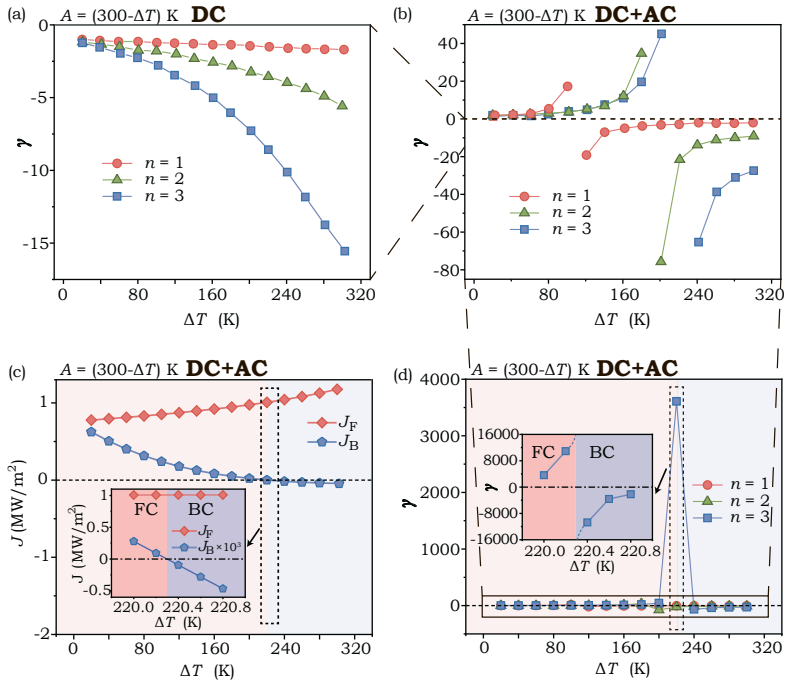

Fig. 3. The thermal rectification ratio γ under the DC and AC+DC heat sources. The thermal rectification ratio γ as a function of ΔT at $n = 1$, 2 and 3 under (a) DC heat sources and (b) AC+DC heat sources in the BC case. (c) The average heat flux density J and (d) the thermal rectification ratio γ as a function of ΔT. The insets show the detail information within a smaller scale of ΔT from 200 K to 220.8 K. Here, A is set as $(300 - \Delta T)$ K, f is set as 50 Hz, $\Delta\varphi$ is set as 0, and TBR is set as $0\,\text{m}^2\cdot\text{K/W}$.

gradient influenced by the AC component of the oscillating heat source and the intrinsic thermal rectification properties of the diode. A comprehensive explanation of this phenomenon is provided in the SM.

Since the $G_{\text{F}}^{\text{eff}}$ can be tuned from negative to positive under AC heat sources, it becomes feasible to design a

thermal rectifier with a nearly infinite thermal rectification ratio by exploiting this phenomenon. To isolate the influence of temperature difference on the thermal rectification, we maintain consistent overlapping intervals between the high and low temperature heat sources. Consequently, in the following simulation, we set $A = (300 - \Delta T)$ K, where ΔT ranges from 0 K to 300 K, while keeping other parameters constant. Under the DC heat sources, the thermal rectification ratio increases with both increased temperature difference and increased highest order of thermal conductivity, as illustrated in Fig. 3(a). Here, a negative thermal rectification ratio indicates that the heat flux reverses with the inversion of the temperature gradient, as defined in Eq. (6). However, for AC heat sources, as depicted in Figs. 3(b) and 3(d), we observe that within certain specific ranges of temperature differences, the thermal rectification ratio diverges exponentially, reaching values as high as 10^5 readily. This occurs because the $G_{\mathrm{F}}^{\mathrm{eff}}$ can be modulated close to 0, resulting in an almost negligible heat flux density J_{B}, as shown in Fig. 3(c). Additionally, at low temperature differences, we also note the thermal rectification ratio is positive, indicating that the heat flux in the heterojunction spontaneously persists in the same direction, regardless of the direction of the temperature gradient. As the temperature difference further increases, the thermal rectification behavior approach that of DC heat sources. Therefore, switching the heat source from DC to AC enables the thermal rectifier to achieve not only an extremely high thermal rectification ratio but also continuous extraction of thermal energy from a system colder than the external heat source. The clarity of this principle, combined with the simplicity of the design, suggests that this powerful thermal rectifier has the potential to significantly impact the strategies of thermal management and thermal control.

Compared with DC heat sources, AC heat sources exhibit obvious advantages in terms of thermal rectification performance and offer more diverse and flexible control

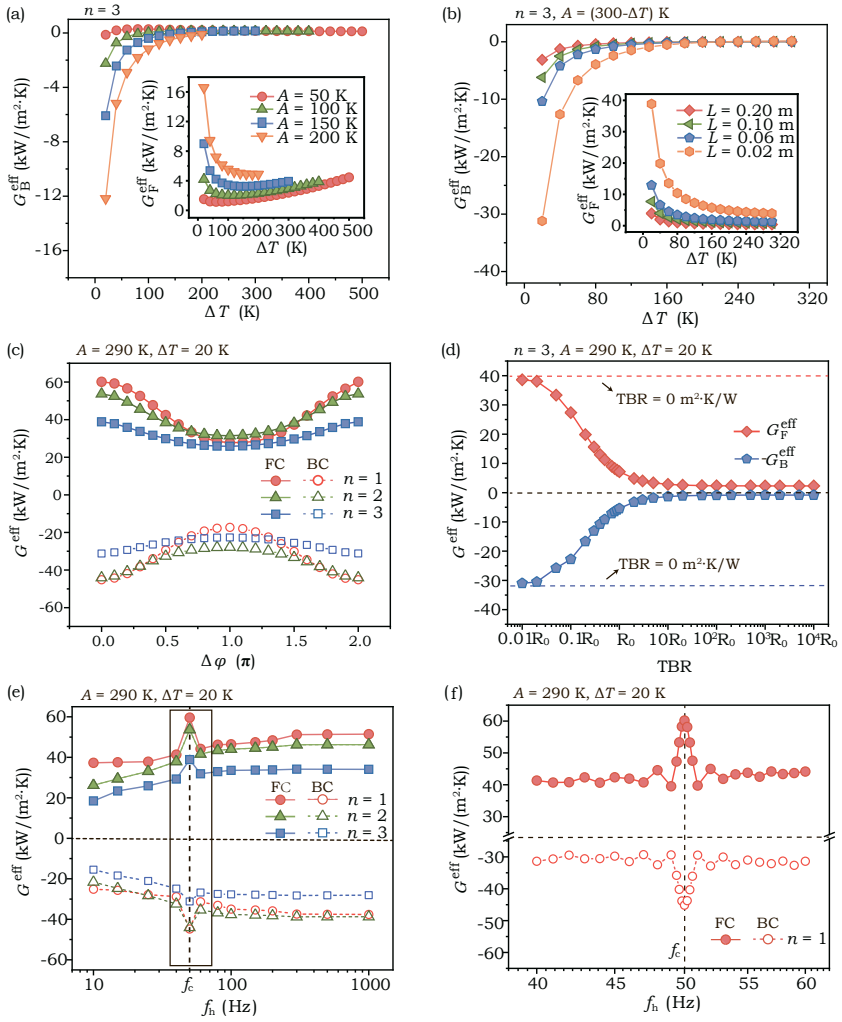

Fig. 4. The modulation of NETC. (a) The influence of amplitude on NETC, with the calculated parameters set as $n = 3$, $L = 0.02$ m, $f = 50$ Hz, TBR $= 0\,\mathrm{m^2{\cdot}K/W}$, and $\Delta\varphi = 0$. (b) The influence of diode length on NETC, with the calculated parameters set as $n = 3$, $A = (300 - \Delta T)$ K, $f = 50$ Hz, TBR $= 0\,\mathrm{m^2{\cdot}K/W}$, and $\Delta\varphi = 0$. (c) The influence of phase difference on NETC, with the calculated parameters set as $n = 3$, $A = 290$ K, $\Delta T = 20$ K, $f = 50$ Hz, and TBR $= 0\,\mathrm{m^2{\cdot}K/W}$. (d) The influence of TBR on NETC, with the calculated parameters set as $n = 3$, $A = 290$ K, $\Delta T = 20$ K, $f = 50$ Hz, and $\Delta\varphi = 0$. (e) The influence of frequency on NETC, with the calculated parameters set as $A = 290$ K, $\Delta T = 20$ K, TBR $= 0\,\mathrm{m^2{\cdot}K/W}$, and $\Delta\varphi = 0$. (f) A zoom-in subfigure (e) at $n = 1$.

strategies. These strategies include variations in the AC amplitude A, thermal difference ΔT, diode length L, thermal boundary resistance TBR, frequency f, and phase difference $\Delta\varphi$. AC amplitude and diode length have similar effects on NETC, as illustrated in Figs. 4(a) and 4(b). Both factors significantly enhance NETC due to the increased intensity of the AC heat source and the reduction of the intrinsic thermal resistance. During thermal transport, the phase difference between the heat sources can deteriorate the NETC, as demonstrated in Fig. 4(c). The phases between heat sources remain coherent, but even at the most decayed π phase, there is still a non-zero NETC, which retains approximately 30% of the strength observed at the zero phase difference. Similarly, the TBR introduces substantial thermal damping into the rectifier, resulting in coherent temperature waves and weakened NETC, as shown in Fig. 4(d). Here R_0 is set as $0.0025\,\mathrm{m^2{\cdot}K/W}$ and the heat flux will approach zero as the TBR increases, hindering the performance of thermal rectification. The impact of the heat source's operating frequency on NETC is particularly notable. Regardless of whether considering NETC or normal ETC, and irrespective of the highest order of thermal conductivity, the optimal intrinsic operating frequency is consistently found to be around 50 Hz, as illustrated in Figs. 4(e) and 4(f). Additionally, we observe several oscillating features near the intrinsic frequency, which we speculated are heavily influenced by the thermal properties and geometric dimensions of the materials.

Based on our investigation, several perspectives for future experiments and practical applications are put forward. In actual design, it is crucial to identify physical systems exhibiting a high thermal rectification ratio. Promising candidates include graphene,[52] VO_2,[42] PE nanofiber,[46] $CaCl_2{\cdot}6H_2O$,[43] $Ge_2Sb_2Te_5$,[41] and thermal metamaterials.[61,62] Concurrently, exploring innovative schemes that maximize the thermal rectification ratio is equally essential. Promising designs of such schemes currently include BC_nN/Graphene heterojunctions,[53] restructured graphene nanoribbons,[63] and suspended monolayer graphene membranes.[50] In these systems, our calculations demonstrate that introducing even a small AC heat source can significantly enhance the unidirectionality of heat flux. Importantly, the thermal rectification ratio of the device can be flexibly modulated by controlling this AC heat source, enabling multifunctional thermal management. For practical implementation, such an AC heat source can be readily realized by combining a heater and a thermoelectric cooler. This straightforward design is easily implementable and readily scalable, facilitating its rapid adoption in various applications. Therefore, such a hybrid active-passive thermal regulation design offers transformative potential for efficient and controllable thermal rectification in various applications.

In conclusion, based on finite element calculations, we designed a thermal diode heterojunction in contact with periodic-oscillating heat sources, and optimized its thermal rectification performance during the transient process. First, we achieved decoupling of heat flux reversal from the average thermal gradient, thereby realizing NETC within this framework. Meanwhile, compared to DC conditions, we observed giant thermal rectification with a thermal rectification ratio significantly exceeding previously reported values. Furthermore, we demonstrated precise control over the ETC, NETC, and thermal rectification by modulating the average temperature gradient, amplitude, frequency, and phase of the periodic-oscillating heat sources. Our work provides guidance for designing and optimizing high-performance thermal diodes in practical applications and opens new research directions for regulating thermal management using AC heat sources.

Acknowledgements. This work was supported by the National Key Research and Development Program of China (Grant No. 2023YFA1407001) and Department of Science and Technology of Jiangsu Province (Grant No. BK20220032).

References

[1] Wang Q, Jiang B, Li B, and Yan Y 2016 *Renew. Sustain. Energy Rev.* **64** 128
[2] Moore A L and Shi L 2014 *Mater. Today* **17** 163
[3] Zhou Y, Anaya J, Pomeroy J, Sun H, Gu X, Xie A, Beam E, Becker M, Grotjohn T A, Lee C, and Kuball M 2017 *ACS Appl. Mater. Interfaces* **9** 34416
[4] Zhou Y, Ramaneti R, Anaya J, Korneychuk S, Derluyn J, Sun H, Pomeroy J, Verbeeck J, Haenen K, and Kuball M 2017 *Appl. Phys. Lett.* **111** 041901
[5] Tian S, Wu T, Hu S, Ma D, and Zhang L 2024 *Appl. Phys. Lett.* **124** 042202
[6] Waldrop M M 2016 *Nature* **530** 144
[7] Yang Y, Zhou Y, Zhang G, Liu F, Li B, Zhao Y, and Zhang L 2024 *Adv. Funct. Mater.* **35** 2412469
[8] Biercuk M J, Llaguno M C, Radosavljevic M, Hyun J K, Johnson A T, and Fischer J E 2002 *Appl. Phys. Lett.* **80** 2767
[9] Song H, Liu J, Liu B, Wu J, Cheng H M, and Kang F 2018 *Joule* **2** 442
[10] Dong Z Y, Zhou Y, Chen X Q, Li W J, Cao Z Y, Luo C, Zhong G H, Peng Q, Wu X, and Chen X J 2022 *Phys. Rev. B* **105** 184301
[11] Zhou Y, Dong Z Y, Hsieh W P, Goncharov A F, and Chen X J 2022 *Nat. Rev. Phys.* **4** 319
[12] Zhou Y, Zhou S, Ying P, Zhao Q, Xie Y, Gong M, Jiang P, Cai H, Chen B, Tongay S, Zhang J, Jie W, Wang T, Tan P, Liu D, and Kuball M 2022 *J. Phys. Chem. Lett.* **13** 3831
[13] Yu Z, Li M, Yang Y, Yu P, Suwardi A, Zhang L, and Zhao Y 2025 *Adv. Electron. Mater.* **11** 2400634
[14] Teo H G, Lee P S, and Hawlader M N A 2012 *Appl. Energy* **90** 309
[15] Santamouris M and Kolokotsa D 2013 *Energy Build.* **57** 74
[16] Chen W Y, Shi X L, Zou J, and Chen Z G 2022 *Small* **6** 2101235
[17] Faghri A 2014 *Faghri, Front. Heat Pipes* **5** 48
[18] Habibi Khalaj A and Halgamuge S K 2017 *Appl. Energy* **205** 1165
[19] Yang Y, Ma D, Zhao Y, and Zhang L 2020 *J. Appl. Phys.* **127** 195301
[20] Yang Y, Zhao Y, and Zhang L 2023 *Appl. Phys. Lett.* **122** 232201
[21] Ahmed H E, Salman B H, Kherbeet A S, and Ahmed M I 2018 *Int. J. Heat Mass Transfer* **118** 129

[22] He Y, Wan S, Zhou S, Huang Z, Chang Y, Yang Y, Gao X, Xu Y, Yang J, Gao S, Ma D, Zhou Y, and Sun H 2025 *Appl. Phys. Lett.* **126** 122201

[23] Zhou Y, Zhou S, Wan S, Zou B, Feng Y, Mei R, Wu H, Shigekawa N, Liang J, Tan P, and Kuball M 2023 *Appl. Phys. Lett.* **122** 082103

[24] Wehmeyer G, Yabuki T, Monachon C, Wu J, and Dames C 2017 *Appl. Phys. Rev.* **4** 041304

[25] Wong M Y, Tso C Y, Ho T C, and Lee H H 2021 *Int. J. Heat Mass Transfer* **164** 120607

[26] Li B, Wang L, and Casati G 2004 *Phys. Rev. Lett.* **93** 184301

[27] Terraneo M, Peyrard M, and Casati G 2002 *Phys. Rev. Lett.* **88** 094302

[28] Peyrard M 2006 *EPL* **76** 49

[29] Wang J, Gong J, McGaughey A J H, and Segal D 2022 *J. Chem. Phys.* **157** 174105

[30] Dmitriev S V, Kuzkin V A, and Krivtsov A M 2023 *Phys. Rev. E* **108** 054221

[31] Ding Y, Zhu G, Shen X, Bai X, and Li B 2022 *Chin. Phys. B* **31** 126301

[32] Li N, Hänggi P, and Li B 2008 *Europhys. Lett.* **84** 40009

[33] Li N, Zhan F, Hänggi P, and Li B 2009 *Phys. Rev. E* **80** 011125

[34] Ren J, Hanggi P, and Li B 2010 *Phys. Rev. Lett.* **104** 170601

[35] Ren J and Li B 2010 *Phys. Rev. E* **81** 021111

[36] Ren J, Liu S, and Li B 2012 *Phys. Rev. Lett.* **108** 210603

[37] Zhang S, Ren J, and Li B 2011 *Phys. Rev. E* **84** 031122

[38] Chen R, Cui Y, Tian H, Yao R, Liu Z, Shu Y, Li C, Yang Y, Ren T, Zhang G, and Zou R 2015 *Sci. Rep.* **5** 8884

[39] Cottrill A L and Strano M S 2015 *Adv. Energy Mater.* **5** 1500921

[40] Fiorino A, Thompson D, Zhu L, Mittapally R, Biehs S A, Bezencenet O, El-Bondry N, Bansropun S, Ben-Abdallah P, Meyhofer E, and Reddy P 2018 *ACS Nano* **12** 5774

[41] Kasali S O, Ordonez-Miranda J, and Joulain K 2020 *Int. J. Heat Mass Transfer* **154** 119739

[42] Kasali S O, Ordonez-Miranda J, and Joulain K 2020 *Int. J. Therm. Sci.* **153** 106393

[43] Kommandur S, Kishore R A, Booten C, Cui S, Wheeler L M, and Vidal J 2021 *Adv. Mater. Technol.* **7** 2101060

[44] Haratoka C, Joulain K, and Ezzahri Y 2023 *Int. J. Heat Mass Transfer* **214** 124452

[45] Kobayashi W, Sawaki D, Omura T, Katsufuji T, Moritomo Y, and Terasaki I 2012 *Appl. Phys. Express* **5** 027302

[46] Shrestha R, Luan Y, Luo X, Shin S, Zhang T, Smith P, Gong W, Bockstaller M, Luo T, Chen R, Hippalgaonkar K, and Shen S 2020 *Nat. Commun.* **11** 4346

[47] Swoboda T, Klinar K, Kitanovski A, and Muñoz Rojo M 2021 *J. Phys. Conf. Ser.* **2116** 012115

[48] Tian H, Xie D, Yang Y, Ren T L, Zhang G, Wang Y F, Zhou C J, Peng P G, Wang L G, and Liu L T 2012 *Sci. Rep.* **2** 523

[49] Shih T M, Gao Z, Guo Z, Merlitz H, Pagni P J, and Chen Z 2015 *Sci. Rep.* **5** 12677

[50] Wang H, Hu S, Takahashi K, Zhang X, Takamatsu H, and Chen J 2017 *Nat. Commun.* **8** 15843

[51] Wang S, Cottrill A L, Kunai Y, Toland A R, Liu P, Wang W J, and Strano M S 2017 *Phys. Chem. Chem. Phys.* **19** 13172

[52] Yang Y, Chen H, Wang H, Li N, and Zhang L 2018 *Phys. Rev. E* **98** 042131

[53] Zhang Y, Pei Q X, Wang C M, Yang C, and Zhang Y W 2018 *J. Phys. Chem. C* **122** 22783

[54] Chen X K, Xie Z X, Zhang Y, Deng Y X, Zou T H, Liu J, and Chen K Q 2019 *Carbon* **148** 532

[55] Wen S, Liu X, Cheng S, Wang Z, Zhang S, and Dang C 2019 *J. Quant. Spectrosc. Radiat. Transfer.* **234** 1

[56] Zhang H, Xiong S, Wang H, Volz S, and Ni Y 2019 *Europhys. Lett.* **125** 46001

[57] Herrera F A, Luo T, and Go D B 2017 *J. Heat Transfer* **139** 091301

[58] Klinar K, Muñoz Rojo M, Kutnjak Z, and Kitanovski A 2020 *J. Appl. Phys.* **127** 234101

[59] Ordonez-Miranda J, Guo Y, Alvarado-Gil J J, Volz S, and Nomura M 2021 *Phys. Rev. Appl.* **16** L041002

[60] Shimokusu T J, Zhu Q, Rivera N, and Wehmeyer G 2022 *Int. J. Heat Mass Transfer* **182** 122035

[61] Chen M, Zhang J, Shen X, Zhu G, and Li B 2024 *Device* **2** 100500

[62] Zhang J, Chen M, Luo W, Wei B, Luo T, Shen X, Li B, and Zhu G 2025 *Nat. Sustain.* **1** 10

[63] Arora A, Hori T, Shiga T, and Shiomi J 2017 *Phys. Rev. B* **96** 165419